

HYDROTHERMAL SYNTHESIS AND OPTICAL PROPERTIES OF UNDOPED AND Eu^{3+} -DOPED ZINC STANNATE NANOCRYSTALS

NGUYEN DUY THIEN

Centre for Materials Science, Faculty of Physics, Hanoi University of Science, 334 Nguyen Trai, Thanh Xuan, Hanoi, Vietnam

NGUYEN NGOC TU

Sao Do University, 24 Thai Hoc, Sao Do, Chi Linh, Hai Duong

NGO NHU VIET

Centre for Materials Science, Faculty of Physics, Hanoi University of Science, 334 Nguyen Trai, Thanh Xuan, Hanoi, Vietnam

NGUYEN DUY PHUONG

Academy of Cryptography Techniques. 141 Chien Thang, Tan Trieu, Thanh Tri, Hanoi

LE VAN VU

Centre for Materials Science, Faculty of Physics, Hanoi University of Science, 334 Nguyen Trai, Thanh Xuan, Hanoi, Vietnam

NGUYEN NGOC LONG

Centre for Materials Science, Faculty of Physics, Hanoi University of Science, 334 Nguyen Trai, Thanh Xuan, Hanoi, Vietnam

Received 24 October 2015

Accepted for publication 24 December 2015

E-mail: duythien_303@yahoo.com

Abstract. *In this work we report a hydrothermal approach for synthesis of zinc stannate (Zn_2SnO_4) nanocrystals. Our research focused on the effect of the molar ratio of initial chemicals, reaction temperature and reaction duration on the phase composition and the fluorescence properties. Structural and optical properties of the final products were investigated in detail. X-ray diffraction analysis indicated that the Zn_2SnO_4 nanocrystals possess face-centered cubic crystal structure. Raman scattering spectra exhibit two characteristic vibrational modes of Zn_2SnO_4 crystals. Optical band gap of Eu^{3+} -doped Zn_2SnO_4 nanocrystals obviously depends on Eu^{3+} content. The room-temperature emission spectra of the undoped Zn_2SnO_4 nanocrystals show two broad bands, while the photoluminescence spectra of Eu^{3+} -doped Zn_2SnO_4 nanocrystals exhibit the emission peaks related to the radiative intra-configurational f-f transitions of Eu^{3+} ions. The absorption transitions within Eu^{3+} ions were observed both in the photoluminescence excitation spectra and in the diffuse reflection spectra.*

Keywords: nanostructures, hydrothermal method, photoluminescence, photoluminescence excitation.

I. INTRODUCTION

Active research in nanotechnology has led to a renewed interest in semiconducting oxide compounds consisting of three components (type $A_2^{II}B^{IV}O_4$), one of which is zinc stannate (Zn_2SnO_4) often called zinc tin oxide. Zn_2SnO_4 has high electron mobility, high electrical conductivity and attractive optical properties which make this compound suitable for a wide range of applications in many fields, such as gas sensors, humidity sensors, negative electrode material for Li-ion batteries, solar cells and photocatalyst for the degradation of organic pollutant. In addition, compared with the binary oxides, the ternary oxides like Zn_2SnO_4 are chemically more stable, making them ideal for applications in extreme conditions, for example, Zn_2SnO_4 were used as flame retardants and smoke inhibitors ([1] and references therein).

By using thermal evaporation technique many researchers have synthesized different Zn_2SnO_4 nanostructures like nanobelts, nanorings, nanowires, nanorods, etc. [2–5]. Zn_2SnO_4 nanoparticles have been successfully synthesized by numerous researchers using hydrothermal method [6]. The hydrothermal method is acknowledged to be a simple and effective way for synthesizing highly crystalline and phase-pure Zn_2SnO_4 nanostructures, which are difficult to obtain through high-temperature solid-state reactions owing to the evaporation of ZnO. Zn_2SnO_4 nanopowders have been also manufactured by other methods such as coprecipitation [7], chemical vapour deposition [8], thermal plasma [9], microwave-assisted solution combustion [10], etc.

Photoluminescence (PL) properties of undoped Zn_2SnO_4 nanostructures have been studied by many investigators [2–4, 7–9]; but the results are different. The reason for this is that the PL of undoped Zn_2SnO_4 is determined by various lattice defects which are strongly dependent on manufacturing technology conditions. On the other hand, Zn_2SnO_4 compound with a wide band gap of about 3.6 eV is expected as a promising host material for doping with optical activators such as rare earth metals. However, to our knowledge, up to now there are only a few works reported on Zn_2SnO_4 doped with Dy^{3+} [7], Eu^{3+} ions [11].

In this work we report a hydrothermal approach for synthesis of pure Zn_2SnO_4 nanocrystals. The effect of the molar ratio of Zn:Sn, NaOH content, hydrothermal temperature and hydrothermal duration on the phase composition has been studied in detail. The Zn_2SnO_4 nanocrystals were doped with Eu^{3+} ions. Structural and optical properties of the undoped and Eu^{3+} -doped Zn_2SnO_4 ($Zn_2SnO_4:Eu^{3+}$) nanocrystals were investigated scrupulously.

II. EXPERIMENTAL

II.1. Sample preparation

Zn_2SnO_4 nanocrystals were synthesized by using a hydrothermal method. The zinc sulphate ($ZnSO_4 \cdot 7H_2O$ 99.99%) and tin tetrachloride ($SnCl_4 \cdot 5H_2O$ 99.99%) were used as the starting materials without further purification, they were dissolved into distilled water to form two transparent solutions, respectively. Then the zinc sulphate solution was slowly added into tin tetrachloride solution. Sodium hydroxide (NaOH) solution was added dropwise into the mixture under magnetic stirring. The final mixture was charged into the Teflon-lined autoclave with 50 % of its capacity. Then the autoclave was put in a drying cabinet and kept at 200 °C for 20 h. After the reaction was terminated, the autoclave was cooled naturally to room temperature. The precipitate was filtered, washed with distilled water, and dried at 70 °C for 6 h. For preparing $Zn_2SnO_4:Eu^{3+}$

nanocrystals, solution of europium nitrate pentahydrate (Eu(NO₃)₃·5H₂O 99.9%) was added into the zinc sulphate solution in appropriate ratio before mixing with the tin tetrachloride solution.

II.2. Characterization

Crystal structure of the synthesized products was analyzed by X-ray diffraction (XRD) using an X-ray diffractometer Siemens D5005, Bruker, Germany, with Cu-Kα₁ (λ = 1.54056 Å) irradiation. Surface morphology of the samples was observed by using a field emission scanning electron microscope (FE-SEM) Nova NANO-SEM-450, FEI. The composition of the samples was determined by an energy-dispersive X-ray spectrometer (EDS) Oxford ISIS 300 attached to a JEOL-JSM5410 LV scanning electron microscope. Raman measurements were carried out by using LabRAM HR 800, Horiba spectrometer with 632.8 nm excitation. PL and photoluminescence excitation (PLE) measurements were performed on a spectrofluorometer Fluorolog FL3-22 Jobin-Yvon-Spex, USA using 450 W xenon lamp as an excitation source. Diffuse reflection spectroscopy measurements were carried out on a VARIAN UV-VIS-NIR Cary 5000 spectrophotometer. The spectra were recorded at room temperature in the wavelength region of 200-900 nm. Absorption spectra of the samples were obtained from the diffuse reflectance data by using the Kubelka-Munk function [12]:

$$F(R) = \frac{(1-R)^2}{2R} = \frac{K}{S}$$

where R , K and S are the reflection, the absorption and the scattering coefficient, respectively.

III. RESULTS AND DISCUSSION

III.1. Crystal structure and morphology

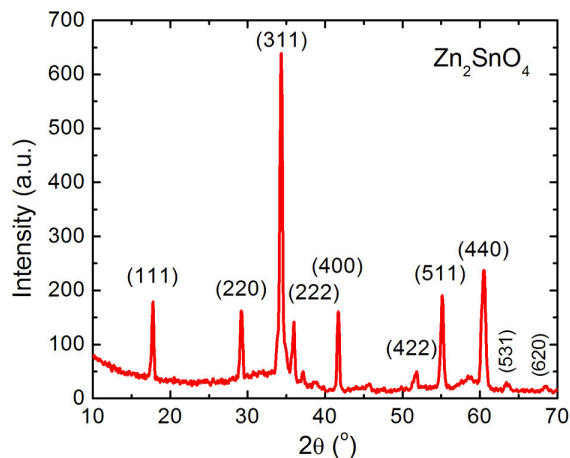


Fig. 1. XRD pattern of Zn₂SnO₄ nanocrystals prepared under the following conditions: the molar ratio of Zn/Sn was 10/6.25, NaOH content was 1 M and reaction was carried out at 200 °C for 20 h.

The XRD pattern of the Zn₂SnO₄ nanocrystals is presented in Fig. 1. The figure shows the position of various diffraction peaks at 2θ values of 17.8°, 29.2°, 34.4°, 35.9°, 41.7°, 51.6°, 60.1°, 62.1°, and 62.1°.

55.1°, 60.4° and 63.4° corresponding to the (111), (220), (311), (222), (400), (422), (511), (440) and (531) diffraction planes of pure face-centered cubic spinel Zn_2SnO_4 , respectively. The lattice constant of the cubic Zn_2SnO_4 nanocrystals was determined from the XRD pattern to be $a = 8.647 \text{ \AA}$ in good agreement with the value of 8.657 \AA of the standard card JCPDS 24-1470.

Based on Scherrer's formula [13], the average size of Zn_2SnO_4 nanocrystals was calculated to be about 76 nm.

Typical EDS spectrum of the Zn_2SnO_4 nanocrystalline powders is shown in Fig. 2. As seen from the figure, the pure Zn_2SnO_4 nanopowders are composed of the elements Zn, Sn and O.

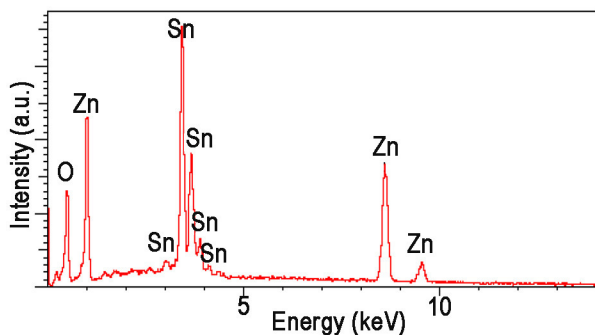


Fig. 2. EDS spectrum of Zn_2SnO_4 nanocrystals.

The FE-SEM image of Zn_2SnO_4 nanopowders depicted in Fig. 3 shows that the Zn_2SnO_4 nanocrystals agglomerated into the bigger octahedra with the size about $1 \mu\text{m}$ and on surface of the octahedra are assembled nanoclusters with the size of 100-400 nm.

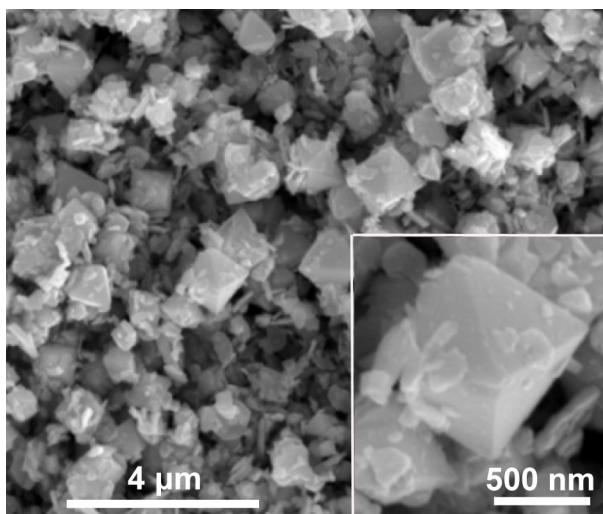


Fig. 3. FE-SEM image of Zn_2SnO_4 nanopowders.

III.2. Effect of hydrothermal conditions on the formation of Zn_2SnO_4 nanocrystals

III.2.1. Effect of molar ratio of Zn/Sn

Fig. 4 shows the XRD patterns of the samples formed by hydrothermal reaction at $200\text{ }^\circ\text{C}$ for 20 h with different molar ratios of Zn/Sn. The concentration of NaOH in this experiment was kept constant and equal to 1 M. As shown in curves (a) and (b) of Fig. 4, at Zn/Sn ratios of 10/8.75 and 10/7.5 (tin content is high), the samples were mixtures of SnO_2 and Zn_2SnO_4 , of which SnO_2 is dominant; while at Zn/Sn ratio of 10/5 (tin content is low), the main phase of the sample was ZnO (curve (d)). The pure Zn_2SnO_4 phase was obtained at Zn/Sn ratio of 10/6.25.

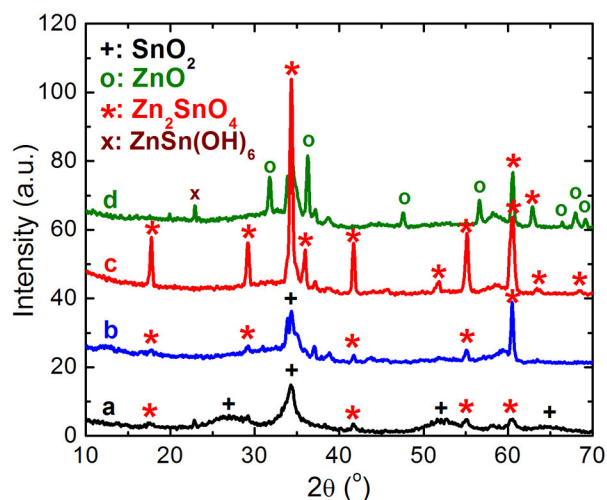


Fig. 4. The XRD patterns of the samples synthesized hydrothermally at $200\text{ }^\circ\text{C}$ for 20 h with 1 M NaOH and different molar ratios of Zn/Sn: (a) 10/8.75; (b) 10/7.5; (c) 10/6.25 and (d) 10/5.

III.2.2. Effect of NaOH concentration

The XRD patterns of the samples prepared hydrothermally at $200\text{ }^\circ\text{C}$ for 20 h with different NaOH concentrations are presented in Fig. 5. Our results show that at a NaOH concentration of 0.5 M, the sample was SnO_2 (curve (a), JCPDS 72-1147). At a NaOH concentration of 1 M, the sample was pure Zn_2SnO_4 (curve (b), JCPDS 24-1470). With further increasing concentration of NaOH to 1.5 and 2.0 M (not shown in Fig. 5), the main phases of sample were ZnO. At a NaOH concentration of 2.5 M, the sample was pure ZnO (curve (c), JCPDS 79-2205). According to Jia Zeng et al. [6], at low concentrations of NaOH, owing to stronger hydrolysis effect of Sn^{4+} ions, colloidal H_2SnO_3 was formed and then in hydrothermal condition this reactant resulted in SnO_2 deposits. When the NaOH concentration increased up, ZnSn(OH)_6 and Zn(OH)_4^{2-} phases were produced and then were combined forming Zn_2SnO_4 precipitates. With further increasing concentration of NaOH, the Zn(OH)_4^{2-} phase decomposed to form ZnO.

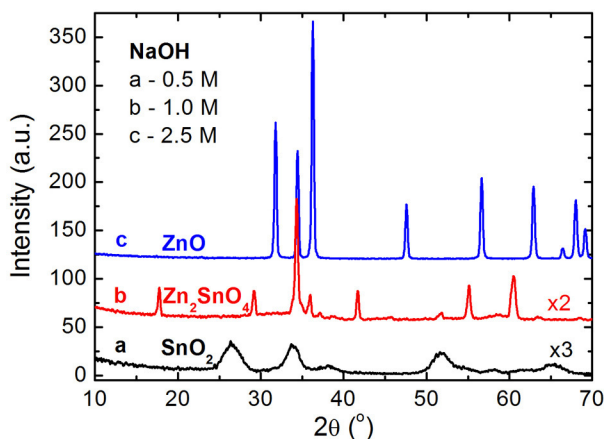


Fig. 5. The XRD patterns of the samples prepared hydrothermally at 200 °C for 20 h with different NaOH concentrations: (a) 0.5 M; (b) 1.0 M; (c) 2.5 M. Zn/Sn molar ratio was 10/6.25.

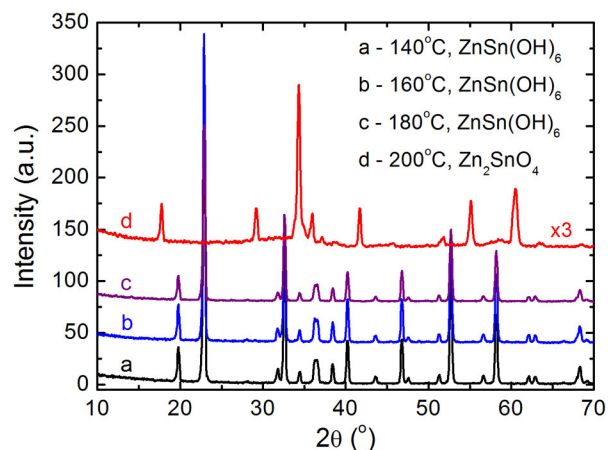


Fig. 6. The XRD patterns of the samples prepared hydrothermally at various temperatures for 20 h with a NaOH concentration of 1 M and a Zn/Sn molar ratio of 10/6.25.

III.2.3. Effect of hydrothermal temperature

Reaction temperature is an important factor for a hydrothermal process. The samples were synthesized at different temperatures and the results are depicted in Fig. 6. At reaction temperatures of 140 °C, 160 °C and 180 °C only the phase of cubic ZnSn(OH)₆ was obtained as shown in Fig. 6 (curves (a)-(c), JCPDS 73-2384). At 200 °C the phase of pure Zn₂SnO₄ was obtained. It is noted that XRD patterns of the samples prepared at the temperatures lower than 200 °C are in agreement with that of both ZnSn(OH)₆ (JCPDS 73-2384) and ZnSnO₃ (JCPDS 11-0274) with cubic lattice structure. So, how to determine whether the samples are ZnSn(OH)₆ or ZnSnO₃? By carrying out thermogravimetric analysis (TGA) and differential thermal analysis (DTA) for

samples, Xiaoxia Xu et al. [14] found that when the temperature is higher than $400\text{ }^\circ\text{C}$, the total mass loss of the as-prepared samples is nearly 20 %, which is in good agreement with that (18.9 %) induced by the decomposition of $\text{ZnSn}(\text{OH})_6$ or the reaction $\text{ZnSn}(\text{OH})_6 \rightarrow \text{ZnSnO}_3 + 3\text{H}_2\text{O}$. Hence, they concluded that the as-prepared samples should be the $\text{ZnSn}(\text{OH})_6$ phase. In our case the samples prepared at the temperatures lower than $200\text{ }^\circ\text{C}$ should be the $\text{ZnSn}(\text{OH})_6$ phase.

III.2.4. Effect of hydrothermal duration

Fig. 7 shows the XRD patterns of the as-prepared samples as a function of reaction duration. When the reaction time reached 5 h, the XRD pattern showed only $\text{ZnSn}(\text{OH})_6$ phase (curve (a)). At the reaction time of 10 h, the $\text{ZnSn}(\text{OH})_6$ phase was less crystallized than the one with 5 h reaction time, and some weak diffraction peaks of Zn_2SnO_4 appeared (curve (b)). With increasing the reaction time to more than 15 h the pure Zn_2SnO_4 phase was observed quite clearly.

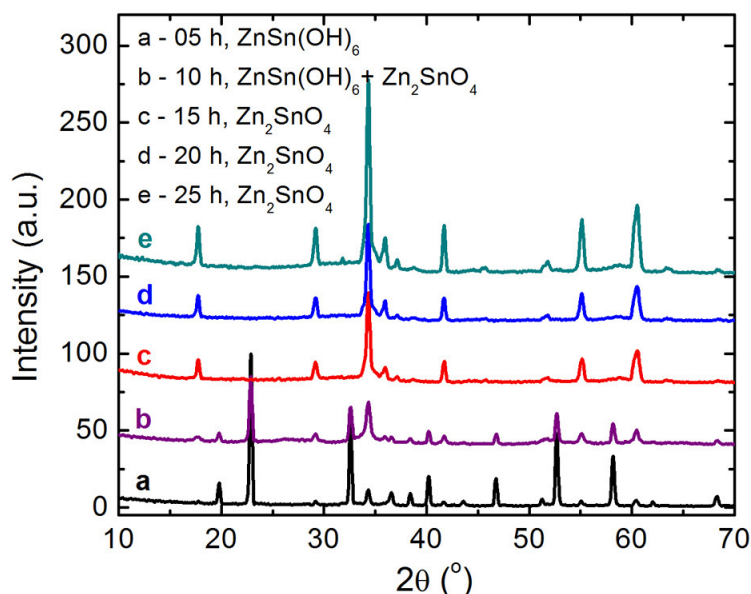


Fig. 7. The XRD patterns of the samples prepared hydrothermally at $200\text{ }^\circ\text{C}$ for different reaction duration with a NaOH concentration of 1 M and a Zn/Sn molar ratio of 10/6.25.

III.3. Raman scattering spectra

Raman spectra of the $\text{ZnSn}(\text{OH})_6$ and Zn_2SnO_4 phases are depicted in Fig. 8. The $\text{ZnSn}(\text{OH})_6$ phase exhibits four Raman modes at 300 , 374 , 438 and 610 cm^{-1} , while Zn_2SnO_4 phase exhibits two modes at 540 and 675 cm^{-1} , which are in agreement with the values reported previously [6, 15]. According to Jia Zeng et al. [6], the four Raman modes for the $\text{ZnSn}(\text{OH})_6$ phase arise from the breathing vibration of the long M-OH bonds and bending modes of the M-OH-M bridging group. The peak at 675 cm^{-1} for Zn_2SnO_4 phase is assigned to stretching vibrations of the short M-O bonds in the MO_6 octahedron. The peak at 540 cm^{-1} is related to internal vibrations of oxygen tetrahedron.

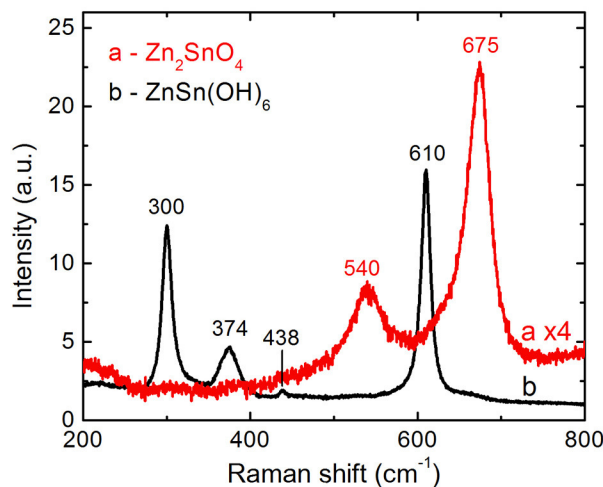


Fig. 8. The Raman spectra of (a) the as-prepared Zn₂SnO₄ nanocrystals and (b) the ZnSn(OH)₆ nanocrystals.

It is found that the position of Raman shift peaks slightly depends upon thermal treatment (Fig. 9 and Table 1). In the as-prepared Zn₂SnO₄ samples Raman shift peaks are located at 540 and 675 cm⁻¹. For the Zn₂SnO₄ samples annealed at 700 °C these peaks are situated at 533 and 665 cm⁻¹, respectively; i.e. are slightly shifted to the lower energy side. At annealing temperatures of 900 °C and 1100 °C, the internal vibrations of oxygen tetrahedron are not changed in position, but the stretching vibrations of the short M-O bonds are shifted to the higher energy side.

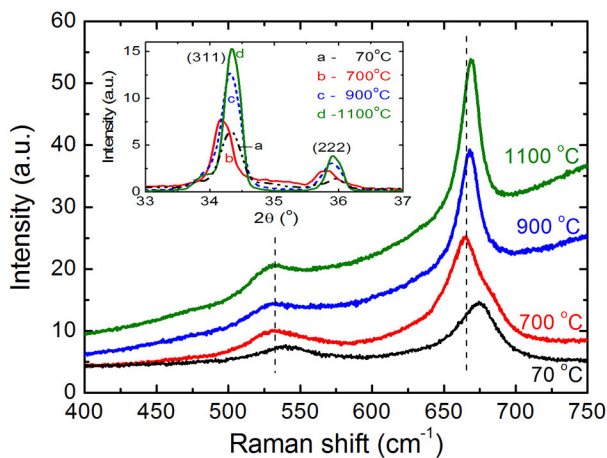


Fig. 9. The Raman spectra of the as-prepared Zn₂SnO₄ nanocrystals and those annealed at 700, 900 and 1100 °C. The inset shows the XRD peaks of (311) and (222) for as-prepared Zn₂SnO₄ nanocrystals and those annealed at 700, 900 and 1100 °C.

It is well known that Raman scattering spectra are closely related with structural characteristics of samples. The XRD analysis showed that XRD pattern of the Zn₂SnO₄ samples undergone

Table 1. Position of the vibrational modes and the (311) and (222) XRD peaks as a function of annealing temperature.

Sample	Vibrations of oxygen tetrahedron (cm ⁻¹)	Vibrations of M-O bonds (cm ⁻¹)	Position of (311) diffraction peak (°)	Position of (222) diffraction peak (°)
As-prepared (dried at 70 °C)	540	675	34.33	35.96
Annealed at 700 °C	533	665	34.18	35.79
Annealed at 900 °C	533	667	34.32	35.89
Annealed at 1100 °C	533	669	34.34	35.94

thermal treatment shifted in the same manner as Raman spectra shifted. The inset of Fig. 9 and Table 1 show the positions of (311) and (222) XRD peaks for as-prepared Zn₂SnO₄ nanocrystals and those annealed at 700, 900 and 1100 °C. In the as-prepared Zn₂SnO₄ samples the (311) and (222) peaks are located at 2θ values of 34.33° and 35.96°, respectively. For the Zn₂SnO₄ samples annealed at 700 °C these peaks are situated at 34.18° and 35.79°, i.e. are somewhat shifted to the lower 2θ side. Further increase of annealing temperature up to 900 °C and 1100 °C leads in shift of these peaks to the larger 2θ side.

The shift of XRD pattern caused by thermal treatment indicates a changing lattice parameter, therefore, bond length; and as a result of this, the vibrational modes are shifted.

III.4. Optical properties

III.4.1. UV-vis absorption spectra

Absorption spectra of the Zn₂SnO₄ samples obtained from the diffuse reflection data by using the Kubelka-Munk (K-M) function $F(R)$ are shown in Fig. 10. The absorption edges of the samples are observed quite obviously. In addition, in the spectrum of 4 % Eu³⁺-doped Zn₂SnO₄ nanocrystals four weak absorption peaks appeared in the spectral region from 350 to 600 nm, which maybe are related with optical transitions within Eu³⁺ ions. The bandgap energy E_g of Zn₂SnO₄ samples can be determined from absorption spectra using following relation [16]:

$$\alpha h\nu = A(h\nu - E_g)^{1/2}$$

where α is the absorption coefficient, $h\nu$ is the incident photon energy, A is a constant and E_g is the band gap of the material.

The plots of $[F(R) \times h\nu]^2$ versus photon energy $h\nu$ for the undoped Zn₂SnO₄ nanocrystals and the Zn₂SnO₄ nanocrystals doped with 1, 2 and 4 % Eu³⁺ are represented in Fig. 11. By extrapolating the straight portion of the graph on $h\nu$ axis at $\alpha = 0$, we found the band gaps of the Zn₂SnO₄ nanocrystals doped with the concentration of 0, 1, 2 and 4 % Eu³⁺ to be 3.699, 4.043, 4.066 and 4.076 eV, respectively. Thus, with increasing Eu³⁺-dopant content from 0 to 4 %, the optical band gap is gradually increased from 3.699 to 4.076 eV. The similar phenomenon was also observed for ZnO doped with any of the group III elements (B, Al, Ga, In) and for many various semiconductors (see, for example, Ref. [17]). This is the well-known Burstein-Moss effect [18, 19]. This phenomenon can be explained as follows. When the Eu impurity atoms of valence 3 substitute for the Zn atoms of valence 2 in Zn₂SnO₄:Eu³⁺ lattice, the Eu atoms become donors, which can give up conduction electrons. With increasing the number of Eu donors, the

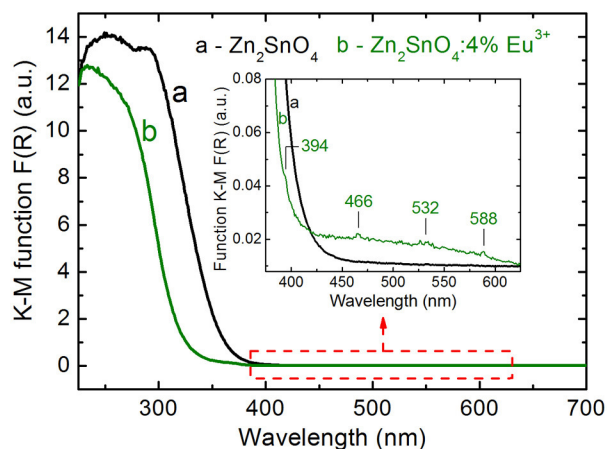


Fig. 10. Kubelka-Munk function proportional to absorption coefficient of the pure and 4 % Eu^{3+} -doped Zn_2SnO_4 nanocrystals. The inset shows some weak absorption peaks in spectral region from 350 to 600 nm.

conduction electron concentration is increased; the Fermi level will rise more and more towards the conduction band. Since the states below the Fermi level are already filled, according to the Pauli Exclusion Principle, the fundamental transitions to the states below the Fermi level are forbidden; hence the optical absorption edge should be shifted to the higher energy side.

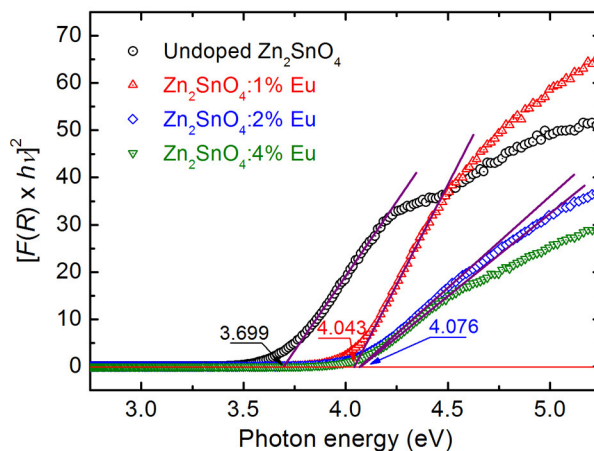


Fig. 11. The plots of $[F(R) \times hv]^2$ versus photon energy hv for the undoped Zn_2SnO_4 nanocrystals and the Zn_2SnO_4 nanocrystals doped with 1, 2 and 4 % Eu^{3+} .

III.4.2. Photoluminescence and photoluminescence excitation spectra

Room temperature PL spectrum under the excitation wavelength of 370 nm for the undoped Zn_2SnO_4 nanocrystals is shown in Fig. 12a. The spectrum consists of two broad emission bands centered at 596 and 662 nm. Broad orange-red emission bands centered at 595-606 and 630-667

nm have been observed in previous reports [4, 5, 8, 9]. These broad emission bands strongly depend on the synthesis condition, and they were usually assigned to the different lattice defects such as oxygen vacancies [5], tin or zinc vacancies [4, 8], the interaction between oxygen vacancies, tin interstitials and oxygen interstitials [8], the residual strain, oxygen vacancies and zinc interstitials [9].

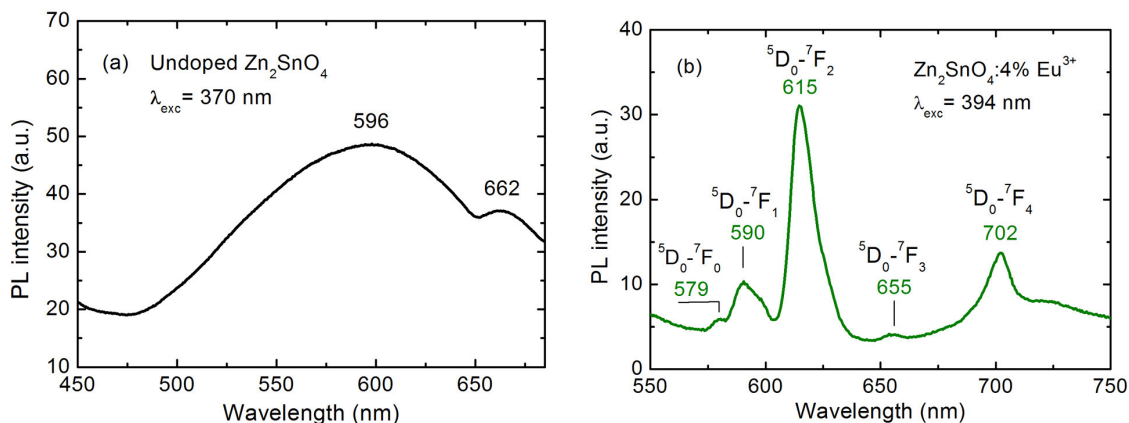


Fig. 12. Room-temperature PL spectra of (a) the undoped Zn_2SnO_4 nanocrystals and (b) the 4 % Eu^{3+} -doped Zn_2SnO_4 nanocrystals.

For Eu^{3+} -doped Zn_2SnO_4 nanocrystals, when the samples were excited by the near-band-edge short wavelengths (347 or 374 nm), in the PL spectra were observed only the broad emission bands centered at 596 and 662 nm, which relate to the mentioned above lattice defects. Only when the samples were excited by the longer wavelengths (394 or 464 nm), in the PL spectra were observed the weak emission peaks related to Eu^{3+} ions. Room temperature PL spectrum under the excitation wavelength of 394 nm for the Zn_2SnO_4 nanocrystals doped with 4 % Eu^{3+} is shown in Fig. 12b. The spectrum exhibits five emission peaks located at 579, 590, 615, 655 and 702 nm, which are attributed to the radiative transitions from the $^5\text{D}_0$ excited state to the $^7\text{F}_0$, $^7\text{F}_1$, $^7\text{F}_2$, $^7\text{F}_3$ and $^7\text{F}_4$ ground states, respectively. Based on these results, it can be deduced that when the samples are excited by the near-band-edge wavelengths, the photogenerated charge carriers recombine mainly via the lattice defects emitting the broad PL bands. If the samples are excited by the longer wavelengths with energies corresponding to the Eu^{3+} ion own excited states, the charge carriers will mainly move from the excited states to the ground state of Eu^{3+} ions emitting the PL peaks which are characteristic of Eu^{3+} ions.

Fig. 13 depicts the PLE spectrum monitored at 615 nm emission line of the Zn_2SnO_4 doped with 4 % Eu^{3+} . The spectrum shows four excitation peaks. The peaks situated at 395, 416, 466 and 527-534 nm are attributed to the absorption transitions from the $^7\text{F}_0$ ground state to the excited states of $^5\text{L}_6$, $^5\text{D}_3$, $^5\text{D}_2$ and $^5\text{D}_1$, respectively. It is interesting to note that the three excitation peaks located at 395, 466 and 534 nm were observed in absorption spectrum as well (see the inset of Fig. 10).

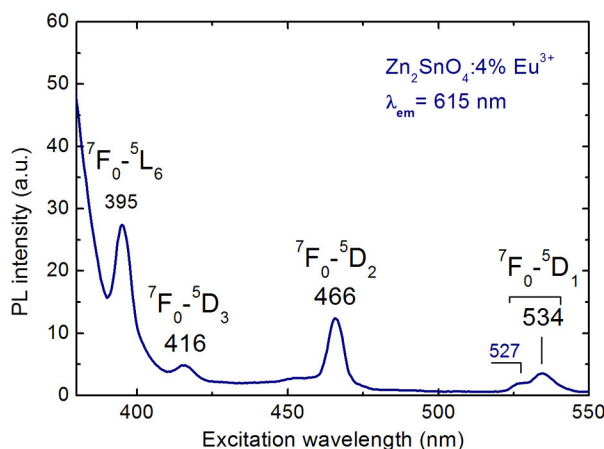


Fig. 13. Typical PLE spectrum monitored at 615 nm emission line of the Zn_2SnO_4 nanocrystals doped with 4 % Eu^{3+} .

IV. CONCLUSION

Zn_2SnO_4 nanocrystals undoped and doped with 1, 2, 3, 4 and 5 mol% Eu have been successfully synthesized by a hydrothermal approach. Optimum technological conditions for synthesis of the Zn_2SnO_4 nanocrystals were as follows: the molar ratio of Zn/Sn was 10/6.25, NaOH concentration was 1 M, reaction temperature and duration was 200 °C and 20 h, respectively. XRD analysis indicated that the Zn_2SnO_4 nanocrystals possess face-centered cubic crystal structure with the lattice constant $a = 8.647 \text{ \AA}$ and the average size of 76 nm. Raman scattering spectra exhibited two vibrational modes at 540 and 675 cm^{-1} which are characteristic of Zn_2SnO_4 crystals. Based on diffuse reflection measurements, it is found that optical band gap of Eu^{3+} -doped Zn_2SnO_4 nanocrystals is gradually increased from 3.699 to 4.076 eV with increasing Eu^{3+} -dopant content from 0 to 4 %. The emission peaks in PL spectra of Eu^{3+} -doped Zn_2SnO_4 nanocrystals are attributed to the radiative transitions from the $^5\text{D}_0$ excited state to the $^7\text{F}_j$ ($j = 0-4$) ground states of Eu^{3+} ions, while the excitation peaks in PLE spectra are assigned to the absorption transitions from the $^7\text{F}_0$ ground state to the excited states of $^5\text{L}_6$, $^5\text{D}_3$, $^5\text{D}_2$ and $^5\text{D}_1$.

ACKNOWLEDGMENT

The authors would like to thank Vietnam National University for financially supporting this research through Project No QGTD 13 04. The authors also thank the VNU project “Strengthening research and training capacity in fields of Nano Science and Technology, and Applications in Medical, Pharmaceutical, Food, Biology, Environmental protection and climate change adaptation in the direction of sustainable development” for providing the equipment to complete this work.

REFERENCES

- [1] Sunandan Baruah and Joydeep Dutta, *Sci. Technol. Adv. Mater.*, **12** (2011) 013004 (18pp).
- [2] J.X. Wang, S.S. Xie, H.J. Yuan, X.Q. Yan, D.F. Liu, Y. Gao, Z.P. Zhou, L. Song, L.F. Liu, X.W. Zhao, X.Y. Dou, W.Y. Zhou, G. Wang, *Solid State Comm.*, **131** (2004) 435-440.
- [3] Lisheng Wang, Xiaozhong Zhang, Xing Liao, Weiguo Yang, *Nanotechnology*, **16** (2005) 2928-2931.

- [4] Jian-Wei Zhao, Li-Rong Qin, Li-De Zhang, *Solid State Comm.*, **141** (2007) 663-666.
- [5] Christina Pang, Bin Yan, Lei Liao, Bo Liu, Zhe Zheng, Tom Wu, Handong Sun, Ting Yu, *Nanotechnology*, **21** (2010) 465706 (4pp).
- [6] Jia Zeng, MuDi Xin, KunWei Li, Hao Wang, Hui Yan, WenJun Zhang, *J. Phys. Chem.*, **C 112** (2008) 4159-4167.
- [7] Shumei Wang, Zhongsen Yang, Mengkai Lu, Yuanyuan Zhou, Guangjun Zhou, Zifeng Qiu, Shufen Wang, Haiping Zhang, Aiyu Zhang, *Mater. Lett.*, **61** (2007) 3005-3008.
- [8] Q.R. Hu, P. Jiang, H. Xu, Y. Zhang, S.L. Wang, X. Jia and W.H. Tang, *J. Alloys and Compd.*, **484** (2009) 25-27.
- [9] Hsiu-Fen Lin, Shi-Chieh Liao, Sung-Wei Hung, Chen-Ti Hua, *Mater. Chem. Phys.*, **117** (2009) 9-13.
- [10] L. C. Nehru, C. Sanjeeviraja, *Nanosci. Nanotechnol.*, **3** (2013) 10-13.
- [11] Zuoling Fu, Hyun Kyoung Yang, Byung Kee Moon, Byung Chun Choi, Jung Hyun Jeong, *Curr. Appl. Phys.*, **9** (2009) 1360-1364.
- [12] Shigeo Shionoya, William M. Yen (Eds.), *Phosphor Handbook edited under the Auspices of Phosphor Research Society*, CRC Press, Boca Raton, Boston, London, New York, Washington DC, 1999, p. 763.
- [13] B.E. Warren, *X-ray Diffraction*, Dover publications, Inc., New York, 1990, p. 253.
- [14] Xiaoxia Xu, Guotao Duan, Yue Li, Hongwen Zhang, Guangqiang Liu, Weiping Cai, *Cryst. Eng. Comm.*, **15** (2013) 6159-6164.
- [15] Yuejiao Chen, Ling Yu, Qing Li, Yan Wu, Qinong Li, Taihong Wang, *Nanotechnology*, **23** (2012) 415501 (10pp).
- [16] E.J. Johnson in: *Semiconductors and Semimetals*, ed. by R.K. Willardson, Albert C. Beer, Vol. 3, Optical Properties of IIIV Compounds, Academic Press, New York and London, 1967, p. 153.
- [17] Jin-Hyun Shin, Dong-Kyun Shin, Hee Young Lee, Jai-Yeoul Lee, Nam-In Cho, Se-Jong Lee, *J. Korean Phys. Soc.*, **55** (2009) 947-951.
- [18] E. Burstein, *Phys. Rev.*, **93** (1954) 632.
- [19] J.I. Pankove, *Optical Processes in Semiconductors*, Prentice-Hall, Inc., Englewood Cliffs, New Jersey, 1971, p. 39.